Multibody System Dynamics **1:** 65–84, 1997.

Biomechanical Model with Joint Resistance for Impact Simulation

M.P.T. SILVA, J.A.C. AMBRÓSIO and M.S. PEREIRA
IDMEC Pólo IST, Avenida Rovisco Pais, 1096 Lisboa Codex, Portugal

(Received: 30 July 1996; accepted in revised form: 19 December 1996)

Abstract. Based on a general methodology using natural co-ordinates, a three-dimensional whole body response model for the articulated human body is presented in this paper. The joints between biomechanical segments are defined by forcing adjacent bodies to share common points and vectors that are used in their definition. A realistic relative range of motion for the body segments is obtained introducing a set of penalty forces in the model rather than setting up new unilateral constraints between the system components. These forces, representing the reaction moments between segments of the human body model when the biomechanical joints reach the limit of their range of motion, prevent the biomechanical model from achieving physically unacceptable positions. Improved efficiency in the integration process of the equations of motion is obtained using the augmented Lagrange formulation. The biomechanical model is finally applied in different situations of passive human motion such as that observed in vehicle occupants during a crash or in an athlete during impact.

Key words: biomechanics, occupant models, injury.

1. Introduction

The development of reliable mathematical models of the human body has been a major challenge for the biomechanics community over the last twenty years [1]. The interest in the simulation of different human actions stems from the need to predict with sufficient accuracy the mechanical behavior of the human body in various conditions of its activity. In fact the simulation of these capabilities have been shown to be useful in different types of applications, including: athletic actions with the aim to improve different sport performances and to optimize the design of sports outfits and equipment; ergonomic studies to assess operating conditions for comfort and efficiency purposes in different aspects of human body interactions with the environment; orthopedics and prosthesis design studies; occupant dynamic analysis for crashworthiness and vehicle safety related research and design.

The biofidelity of modern human body representations is very sensitive to the type of mathematical formalisms used and their capability of supporting the efficient description of the biomechanical aspects of the human activities under analysis. In many situations, such as the case of athletic motions and occupants in vehicle crash design studies, “gross-motion” simulators [2] are preferred to the more expensive finite element based models. In the “gross-motion” simulators the different segments of the human body are typically represented within the

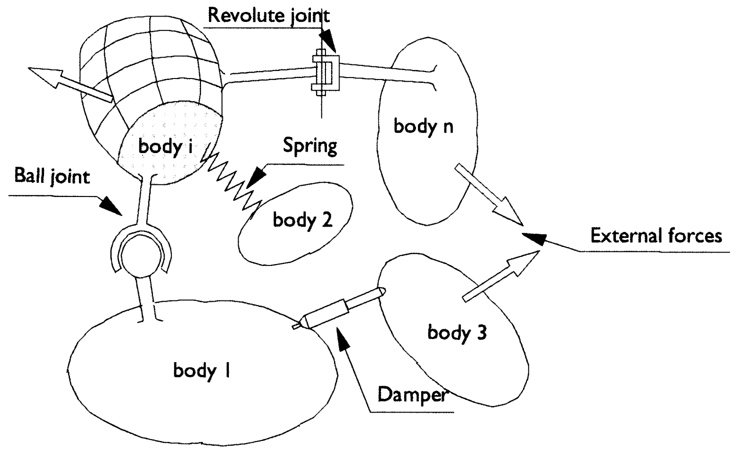

Figure 1. General multibody system.

framework of multibody systems by a set of rigid bodies connected by different types of joints and actuators with a varying degree of complexity. Such detailed biomechanic models are combined in a "gross-motion" simulation tool which can be used with greater efficiency in different situations [3–6].

The multibody dynamics formulations used in this work are briefly introduced. A set of natural co-ordinates are used in the description of the position of each body in the system. The dynamic equations of motion are then obtained using the augmented Lagrangean formulation. The computer models of the human body include different features, namely: a complex system of generalized forcing functions representing adequate reactions between different segments of the human body; intrusion effects and contact-impact capabilities.

Some applications of this complex model are presented in typical passive human motion cases such as the analysis of occupant motion in different vehicle crash scenarios and the simulation of a side tackle of an athlete often observed in rugby and American football. The biofidelity of such models is best illustrated in the computer animation of the resulting gross motion events of the different simulations.

2. Multibody Equations of Motion with Natural Coordinates

2.1. General Multibody System

A multibody system is a collection of rigid and/or flexible bodies joined together by kinematic joints and acted by forces, as depicted by Figure 1. The forces applied over the system components may be the result of spring, dampers or actuators, devices or external applied forces describing, gravitational forces, seat belts, contact-impact forces, or even complex biomechanical or mechanical joints.

Regardless of the system being modeled, it is necessary to describe systematically and efficiently its equations of motion. Among the different sets of co-ordinates,

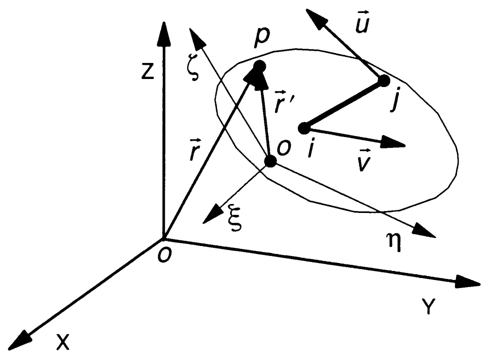

Figure 2. Inertial and local co-ordinate systems.

that can be chosen to describe the system, the natural co-ordinates provide a comprehensive form of integrating efficiently different system features with generality [7–10].

2.2. Equations of Motion of a Rigid Body

With the use of natural co-ordinates a rigid body is described by a collection of points and vectors. In Figure 2, a basic rigid body defined by two basic points and two non-coplanar unit vectors is represented. Other rigid bodies defined by an arbitrary large number of points and vectors may be obtained from this basic body by means of a co-ordinate transformation [7, 8].

Let the rigid body have a local reference frame (ξ, η, ζ) rigidly attached to it and with an origin located in point o. Note that the origin of the body fixed referential is not necessarily its center of mass. Let the principle of the virtual power be used to derive the equations of motion of the rigid body. The position vector $\mathbf{r}$ for a point is described as a function of the co-ordinates of the basic points and vectors of the rigid body

$$\mathbf{r} = \mathbf{C}\mathbf{q}_e, \tag{1}$$

where $\mathbf{C}$ is a transformation matrix independent of the motion of the body and therefore constant in time

$$\mathbf{C} = [(1 - c_1)\mathbf{I}_3 \quad c_1\mathbf{I}_3 \quad c_3\mathbf{I}_3 \quad c_3\mathbf{I}_3], \tag{2}$$

where c_1, c_2 and c_3 are the components of $(\mathbf{r} - \mathbf{r}_i)$ described in the local referential defined by $(\mathbf{r}_j - \mathbf{r}_i)$, $\mathbf{u}$ and $\mathbf{v}$. $\mathbf{I}_3$ is a 3×3 identity matrix and $\mathbf{q}_e = [\mathbf{r}_i^T \ \mathbf{r}_j^T \ \mathbf{u}^T \ \mathbf{v}^T]^T$ is the vector of co-ordinates of the basic points and vectors with respect to the global reference frame xyz. Differentiating Equation (1) with respect to time results in the velocity and acceleration equations for point P:

$$\dot{\mathbf{r}} = \mathbf{C}\dot{\mathbf{q}}_e, \tag{3}$$

$$\ddot{\mathbf{r}} = \mathbf{C}\ddot{\mathbf{q}}_e. \tag{4}$$

The virtual power of the inertia forces for the rigid body is expressed as:

$$W^* = -\dot{\mathbf{q}}_e^{*T} \left(\int_\Omega \rho \mathbf{C}^T \mathbf{C} \, \mathrm{d}\Omega \right) \ddot{\mathbf{q}}_e, \tag{5}$$

where ρ is the mass density and Ω the volume of the rigid body. It must be noted that virtual velocity vector $\dot{\mathbf{q}}_e^*$ and the acceleration vector for the basic vectors and points $\ddot{\mathbf{q}}_e$ are independent of the body volume. The body mass matrix is

$$\mathbf{M} = \int_\Omega \rho \mathbf{C}^T \mathbf{C} \, \mathrm{d}\Omega. \tag{6}$$

Integrating Equation (6) leads to the 12×12 rigid body mass matrix

$$\mathbf{M} = \begin{bmatrix} (m - 2ma_1 + z_{11})\mathbf{I}_3 & (ma_1 + z_{11})\mathbf{I}_3 & (ma_2 + z_{12})\mathbf{I}_3 & (ma_3 + z_{13})\mathbf{I}_3 \\ (ma_1 + z_{11})\mathbf{I}_3 & z_{11}\mathbf{I}_3 & z_{12}\mathbf{I}_3 & z_{13}\mathbf{I}_3 \\ (ma_2 + z_{21})\mathbf{I}_3 & z_{21}\mathbf{I}_3 & z_{22}\mathbf{I}_3 & z_{23}\mathbf{I}_3 \\ (ma_3 + z_{31})\mathbf{I}_3 & z_{31}\mathbf{I}_3 & z_{32}\mathbf{I}_3 & z_{33}\mathbf{I}_3 \end{bmatrix}, \tag{7}$$

where m is the rigid body mass, z_{ij} are coefficients related to the inertia tensor and a_i the components of the static moment of the rigid body [7]. This mass matrix is invariant.

The mass matrix of bodies defined with different sets of basic points and vectors is obtained from this matrix after a proper co-ordinate transformation. This transformation corresponds to relate the position of the new points and vectors as a function of the points and vectors of the basic rigid body just described [7].

Concentrated forces can be applied in a generic point of the rigid body, other than a basic point, as described by Figure 3a. The case of an applied moment, as depicted by Figure 3b, is described by a force binary where the two opposite forces act in a plane perpendicular to the applied moment.

The concentrated force $\mathbf{f}$ applied on point P of a rigid body is described by a generalized force $\mathbf{g}_e$, applied to the basic points and vectors of that body. The relation between these forces is obtained using the equivalence between their virtual work

$$\delta W = \delta \mathbf{r}_p^T \mathbf{f} = \delta \mathbf{q}_e^T \mathbf{g}_e. \tag{8}$$

Vector $\mathbf{r}_p$, representing the position of point P, is related with the basic co-ordinates by Equation (1). Comparing the terms of the resulting equations, it is found that:

$$\mathbf{g}_e = \mathbf{C}_p^T \mathbf{f}. \tag{9}$$

An applied moment is described here by a torque $\mathbf{m}$ given by two non-collinear and opposite forces $\mathbf{f}$ related by

$$\mathbf{m} = \tilde{\mathbf{u}}_m \mathbf{f}, \tag{10}$$

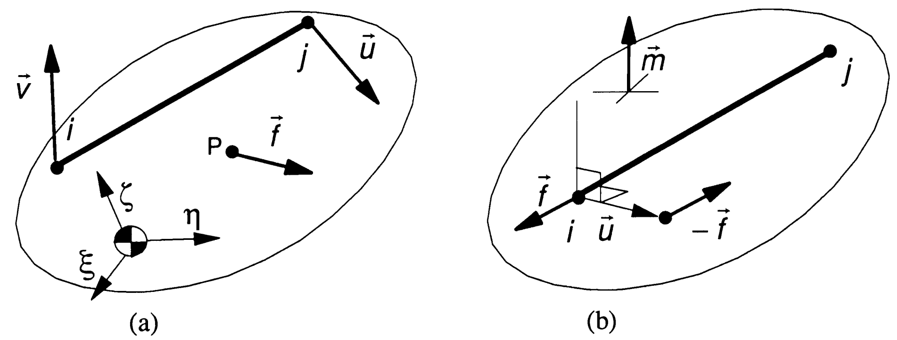

Figure 3. Applied forces and moments: (a) External force; (b) Applied moment.

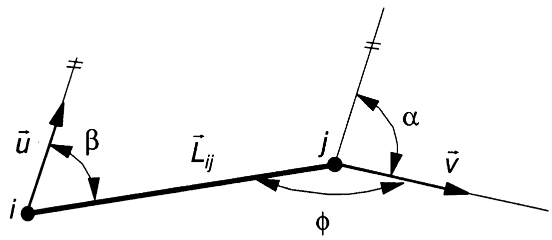

Figure 4. Kinematic constraints defining a rigid body.

where $\mathbf{u}_m$ is a unit vector defined as

$$\mathbf{u}_m = -\frac{\tilde{\mathbf{m}}(\mathbf{r}_j - \mathbf{r}_i)}{\|\tilde{\mathbf{m}}(\mathbf{r}_j - \mathbf{r}_i)\|} \; ; \tag{11}$$

after some algebraic manipulations it is found that the generalized force describing the applied moment is written as

$$\mathbf{g}_e = (\mathbf{C}_i^T + \mathbf{C}_{i+u_m}^T)\mathbf{f}. \tag{12}$$

If the applied moment has the same direction of $(\mathbf{r}_j - \mathbf{r}_i)$ the direction of $\mathbf{u}_m$ must be chosen to be perpendicular to $(\mathbf{r}_j - \mathbf{r}_i)$ instead of using Equation (11).

In order for the set of co-ordinates with the positions of the basic points and vectors to represent a rigid body their co-ordinates cannot be independent of each other, i.e., 6 independent kinematic relations between the 12 co-ordinates describing the points and vectors need to be setup in order to have the 6 degrees of freedom of a rigid body. As depicted by Figure 4, the kinematic constraints, describing the conditions of constant vector length and constant angle between vectors, are

$$\mathbf{r}_{ij}^T\mathbf{r}_{ij} - L_{ij}^2 = 0, \tag{13a}$$

$$\mathbf{u}^T\mathbf{u} - 1 = 0, \tag{13b}$$

$$\mathbf{v}^T\mathbf{v} - 1 = 0, \tag{13c}$$

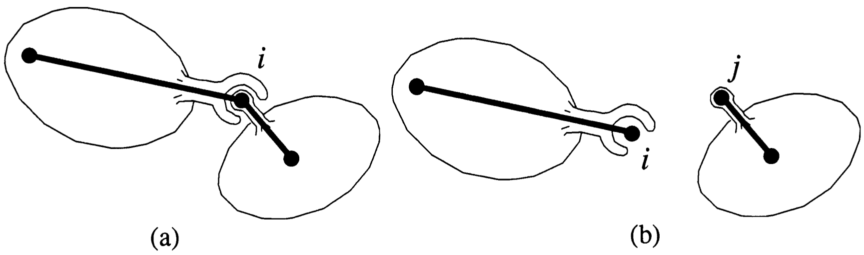

Figure 5. Spherical joint defined by (a) sharing a common point, (b) two different points.

$$\mathbf{r}_{ij}^T\mathbf{u} - L_{ij}\cos\beta = 0, \tag{13d}$$

$$\mathbf{r}_{ij}^T\mathbf{v} - L_{ij}\cos\phi = 0, \tag{13e}$$

$$\mathbf{u}^T\mathbf{v} - \cos\alpha = 0, \tag{13f}$$

where the relations $\mathbf{r}_{ij} = (\mathbf{r}_j - \mathbf{r}_i)$ and $L_{ij} = \|\mathbf{r}_j - \mathbf{r}_i\|$ are used. These kinematic contraints are written in a compact form as

$$\boldsymbol{\Phi}(\mathbf{q}, t) = \mathbf{0}. \tag{14}$$

Differentiating Equation (14) twice with respect to time yields the acceleration equation

$$\boldsymbol{\Phi}_{\mathbf{q}}\ddot{\mathbf{q}} = \boldsymbol{\gamma}. \tag{15}$$

Equation (14) is added to the equations of motion of the rigid body using the Lagrange multiplier technique and solved together with Equation (15) yielding

$$\begin{bmatrix} \mathbf{M} & \boldsymbol{\Phi}_{\mathbf{q}}^T \\ \boldsymbol{\Phi}_{\mathbf{q}} & \mathbf{0} \end{bmatrix} \begin{bmatrix} \ddot{\mathbf{q}} \\ \boldsymbol{\lambda} \end{bmatrix} = \begin{bmatrix} \mathbf{Q} \\ \boldsymbol{\gamma} \end{bmatrix}. \tag{16}$$

Notice that when other co-ordinates are used to describe the rigid body equations of motion the kinematic constraints do not appear in the single body equations. However, those formulations use rotational co-ordinates to describe the rigid body motion.

2.3. Equations of Motion for a Multibody System

One of the advantages of the formulation used here is that many of the most common kinematic constraints used between different bodies are already verified in the definition of the rigid bodies. This situation is described in Figure 5a where point i is used in the definition of both bodies and implicitly the spherical joint definition does not require any extra equations. The most common formulations would require an extra set of equations to be defined between points i and j of Figure 5b to describe the same joint.

The multibody system equations of motion are obtained by evaluating Equation (16) for all individual bodies of the system. If new kinematic constraints are required, these must be added to the resulting equations using Lagrange multipliers. The constrained equations of motion solved using the augmented Lagrangian method [11, 12] and integrated using the Gear method [13].

3. Contact-Impact Force Model

In order to have a reliable model for the contact/impact for the system components or for the human body special attention has to be given to the numerical description of the contact forces. The model must include the information on the contact speed and compliance and their relation to the geometry and material properties of the bodies in contact. Moreover, the contact force model must be suitable for a stable integration of the multibody equations of motion. These characteristics are obtained with a continuous contact force model [14].

Let the contact force between a rigid body and the surface of an object or another body be a function of a pseudo-penetration and a pseudo-velocity of penetration

$$\mathbf{f}_{s,i} = (K\delta^n + D\dot{\delta})\mathbf{u}, \tag{17}$$

where D is a damping coefficient and K is a generalized stiffness coefficient which depends on the geometry of the surfaces in contact and their material properties. The damping coefficient, which introduces the hysteresis damping for the surfaces in contact can be shown to be a function of impact velocity $\dot{\delta}^{(-)}$, relative stiffness of the contacting surfaces and restitution coefficient e. The contact force is finally given by

$$\mathbf{f}_{s,i} = K\delta^n \left[1 + \frac{3(1-e^2)}{4}\,\frac{\dot{\delta}}{\dot{\delta}^{(-)}}\right]\mathbf{u}. \tag{18}$$

Note that the restitution coefficient e reflects the type of impact (for a fully elastic contact $e = 1$ while for a fully plastic contact $e = 0$). This equation is valid for impact velocities lower than the propagation speed of elastic waves across the bodies, i.e., $\dot{\delta}^{(-)} \leq 10^{-5}\sqrt{E/\rho}$ [15]. In all applications considered here this criterion is fulfilled.

4. Biomechanical Model

In this section a three-dimensional, whole body response, biomechanical model of the human body, based on the model presented in SOMLA [3] is presented. This model is developed within a general purpose multibody code that uses the methodologies described in the previous sections. All the information required to assemble the equations of motion of the model is hold in a database created for

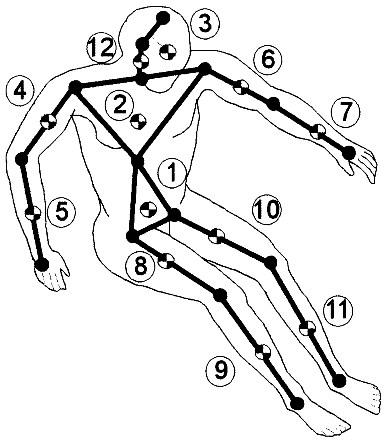

Figure 6. Three-dimensional biomechanical model.

Table I. Kinematic joints description.

Joint no.	Type	Description
1	Spherical	Back, between 12th thoracic and 1st lumbar vertebrae.
2	Spherical	Torso–Neck, between 7th cervical and 1st thoracic vertebrae.
3–5	Spherical	Shoulder.
4–6	Revolute	Elbow.
7–9	Spherical	Hip.
8–10	Revolute	Knee.
11	Revolute	Head–Neck, at occipital condyles.

the purpose. The necessary information is basically the mass, the dimension, the principal moments of inertia and the center of mass location of each rigid body. Using this database, human subjects with different sizes and masses can be easily modeled. In this work, data is presented concerning two biomechanical models: the 50% Anthropomorphic Dummy and the 50% Human Male.

4.1. Model Description

The model is described using 12 rigid bodies interconnected by 11 kinematic joints, as shown in Figure 6. The kinematic joints used in the model are of two types: spherical and revolute joints. The hand and foot segments were not included in the model because their influence in the prediction of injuries resulting from the crash phenomena is not very relevant.

The 12 rigid bodies are defined using 16 basic points and seventeen unit vectors that are located at the articulations and extremities. A total number of 99 natural co-ordinates are used. The kinematic processing of these 12 rigid bodies generates a total number of 70 kinematic constraints, providing the biomechanical model with

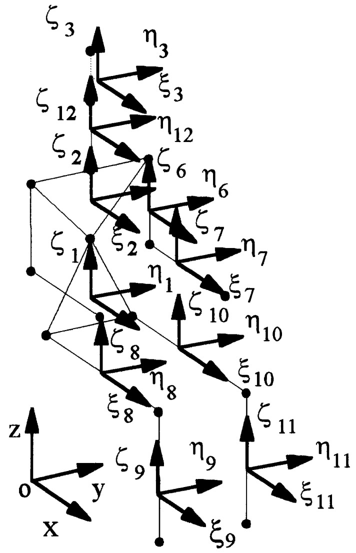

Figure 7. Global and local reference frames.

29 degrees of freedom. In Table I, the description and location of the 11 kinematic joints is presented.

4.2. DIMENSIONS, MASSES AND MOMENTS OF INERTIA

In this section the principal characteristics of the 12 rigid bodies are presented. A local reference frame is rigidly attached to the center of mass of each body, as shown in Figure 7. The spatial orientation of these reference frames is given in such a way that the moments of inertia required in the definition of each body, are all principal moments.

4.2.1. *Rigid Body Dimensions*

The principal dimensions of the model are represented in Figure 8. These are, in most cases, effective link-lengths between two kinematic joints instead of standard anthropometric dimensions based on external measurements. Their numerical values are presented in Table II.

4.2.2. *Masses and Center of Mass Locations*

The center of mass location is given by the distance of the center of mass from the nearest joint, as shown in Figure 8. The mass and center of mass locations of the 12 rigid bodies are presented in Table III.

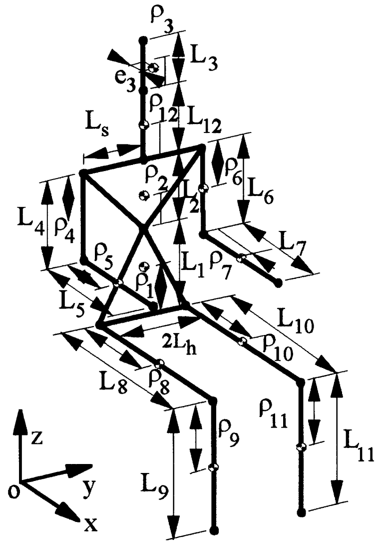

Figure 8. Rigid body dimensions and center of mass location.

Table II. Rigid body dimensions [3].

Body no.	50% Human Male L_i [m]	50% Anthropomorphic Dummy L_i [m]
1	0.240	0.274
2	0.333	0.295
3	0.216	0.212
4–6	0.295	0.287
5–7	0.376	0.338
8–10	0.434	0.419
9–11	0.467	0.457
12	0.130	0.124

4.2.3. *Moments of Inertia*

The moments of inertia with respect to the three principal axes of each rigid body are shown in Table IV. The moments of inertia with respect to the local directions ξ and ζ appear respectively in the form $I_{\xi\xi}/I_{\eta\eta}$ and $I_{\zeta\zeta}/I_{\eta\eta}$. In order to obtain the correct values of $I_{\xi\xi}$ and $I_{\zeta\zeta}$, it is necessary to multiply those ratios by the value of $I_{\eta\eta}$.

4.3. Model Contact Surfaces

A set of contact surfaces is defined for the calculation of the external forces exerted on the model by the seat cushions and the floor. These surfaces are ellipsoids and

Table III. Mass and center of mass location for each rigid body [3].

Body no.	50% Human Male		50% Anthropomorphic Dummy	
	Mass [kg]	ρ_i [m]	Mass [kg]	ρ_i [m]
1	14.198	0.064	15.695	0.119
2	24.948	0.193	16.330	0.166
3	4.241	0.141	4.581	0.161
4–6	1.991	0.153	2.200	0.120
5–7	1.842	0.180	2.200	0.159
8–10	9.843	0.215	9.843	0.212
9–11	4.808	0.230	4.305	0.279
12	1.061	0.049	0.898	0.062
L_s	–	0.161	–	0.161
L_h	–	0.094	–	0.094
e	–	0.051	–	0.051

Table IV. Principal moments of inertia for each rigid body [3].

Body no.	50% Human Male			50% Anthropomorphic Dummy		
	$I_{\xi\xi}/I_{\eta\eta}$	$I_{\eta\eta}$ [kg.m^2]	$I_{\zeta\zeta}/I_{\eta\eta}$	$I_{\xi\xi}/I_{\eta\eta}$	$I_{\eta\eta}$ [kg.m^2]	$I_{\zeta\zeta}/I_{\eta\eta}$
1	1.950	3.482×10^{-4}	1.950	3.053	2.224×10^{-4}	3.053
2	0.663	9.628×10^{-4}	0.517	2.354	2.710×10^{-4}	1.836
3	1.382	5.824×10^{-5}	1.171	1.034	7.784×10^{-5}	0.876
4–6	1.100	3.512×10^{-5}	0.183	0.977	3.951×10^{-5}	0.163
5–7	0.133	7.433×10^{-4}	0.866	0.092	5.414×10^{-5}	1.054
8–10	0.303	4.126×10^{-4}	0.832	0.350	3.570×10^{-4}	0.961
9–11	0.972	3.424×10^{-4}	0.432	0.933	2.910×10^{-4}	0.508
12	0.980	5.560×10^{-6}	0.030	0.980	5.180×10^{-6}	0.030

cylinders and are depicted in Figure 9. In Table V, the main dimensions of these surfaces are presented.

5. Joint Resistance

In this section, a methodology to model the joint resistance torques, is presented. These torques simulate the muscle passive behavior and they also prevent the biomechanical model reaching physically unacceptable positions. The joint resistance torque are modeled using a viscous torsional damper and a non-linear torsional spring, that are located in each kinematic joint, like in Figure 10 for the elbow joint.

Table V. Dimensions of contact surfaces.

Body no.	50% Human Male R_i [m]	50% Anthropomorphic Dummy R_i [m]
1	0.102	0.114
2	0.127	0.114
3	0.095	0.0874
4–6	0.053	0.050
5–7	0.042	0.047
8–10	0.083	0.079
9–11	0.057	0.058
12	0.051	0.051

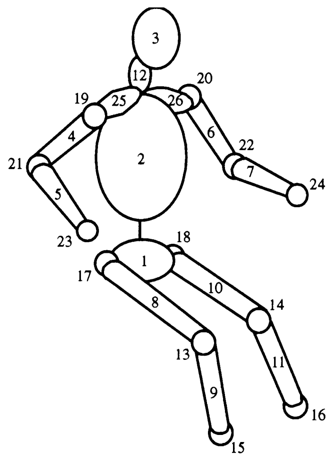

Figure 9. Representation of contact surfaces.

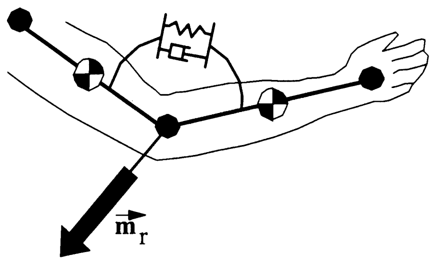

Figure 10. Joint resistance torque modeled using a system of non-linear spring and damper.

5.1. Viscous Torsional Damper

This element is included in order to permit some energy dissipation. The torsional damper has a small constant coefficient j_i being the total damping torque at each joint given by the expression

$$\mathbf{m}_{d_i} = -j_i \dot{\boldsymbol{\beta}}_i, \tag{19}$$

where $\dot{\boldsymbol{\beta}}_i$ is the relative angular velocity vector between the two bodies interconnected by that joint and the index i denotes the joint number. As one can see from Equation (19), the torque $\mathbf{m}_{d_i}$ and the vector $\dot{\boldsymbol{\beta}}_i$ have opposite directions meaning that this torque acts to resist the motion of the joint.

5.2. Non-Linear Torsional Spring

The contribution of the non-linear spring has two terms. The first one is a resisting torque $\mathbf{m}_{r_i}$ that acts to resist the motion of the joint. For the dummy joint, this torque has a constant value and it is applied to the whole range of the joint motion. For the human joint this torque has an initial value which drops to zero after a small angular displacement from the joint initial position [16]. In both cases, this torque has a direction that is opposite to the direction of the relative angular velocity vector between the two bodies interconnected by that joint, that is

$$\mathbf{m}_{r_i} = -m_{r_i} \dot{\boldsymbol{\beta}}_i \|\dot{\boldsymbol{\beta}}_i\|^{-1}. \tag{20}$$

The second term is a penalty resisting torque $\mathbf{m}_{p_i}$. This torque is null during the normal joint rotation but it increases rapidly, from zero until a maximum value, when the two bodies interconnected by that joint, achieve physically unacceptable positions. In the following section a methodology for the calculation of the value of this torque is presented.

5.2.1. *Calculation of the Penalty Resisting Torque*

In this section, the methodology to calculate the penalty torque is applied to the shoulder joint because it is the most mobile of all the joints of the human body. Nevertheless, this is a general methodology that can be applied to any joint of the biomechanical model.

Considering Figure 11, the first step for the calculation of the penalty torque is the construction of the cone of circumduction, this is, the cone of feasible motion. This cone is centered on the shoulder and describes a sector of accessibility, wherein the arm can move without displacement of the upper and lower torso. The range of motion is obtained from [17].

A local reference frame is constructed and rigidly attached to the shoulder joint (points 3 and 5), as shown in Figure 12. The vectors defining the local axes $\mathbf{u}_\xi$ and

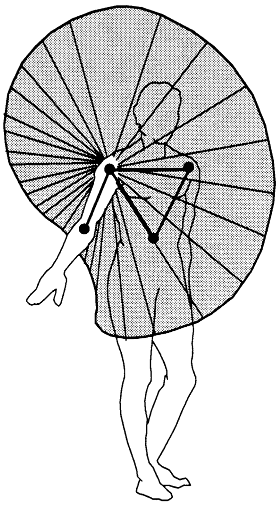

Figure 11. Cone of circumduction for the shoulder joint.

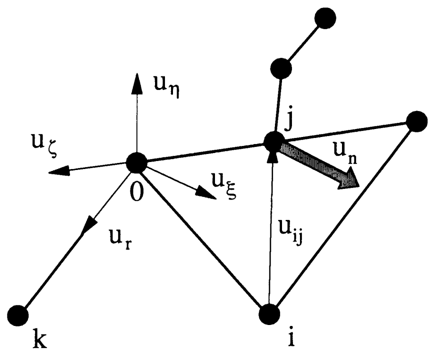

Figure 12. Local reference frame for the shoulder joint.

$\mathbf{u}_\eta$ are built using basic points and unit vectors that were used in the definition of the upper torso rigid body, i.e.

$$\mathbf{u}_\xi = \mathbf{u}_n \tag{21}$$

and

$$\mathbf{u}_\eta = \frac{\mathbf{r}_j - \mathbf{r}_i}{\|\mathbf{r}_j - \mathbf{r}_i\|} \; . \tag{22}$$

The third base vector is calculated as the result of the cross product of the first two:

$$\mathbf{u}_\zeta = \tilde{\mathbf{u}}_\xi \mathbf{u}_\eta . \tag{23}$$

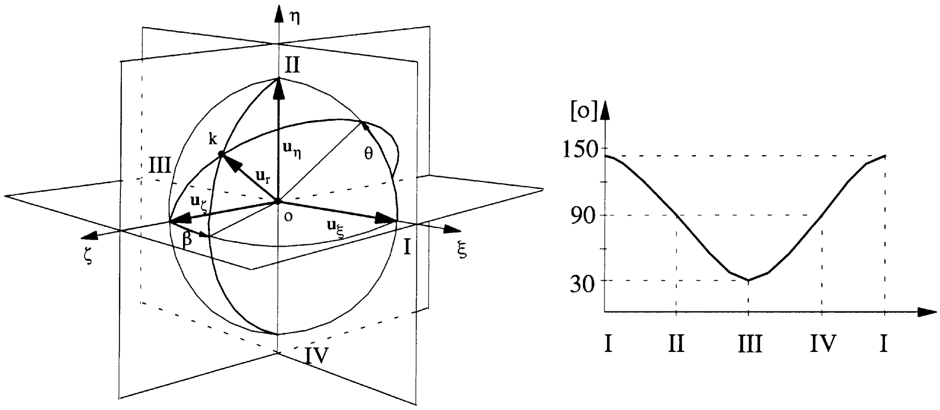

Figure 13. Longitude and latitude angles and interpolation curve for the shoulder joint.

After the construction of this reference frame, a fourth vector is introduced with the same direction of the upper arm and is expressed using the two basic points belonging to this body:

$$\mathbf{u}_r = \frac{\mathbf{r}_k - \mathbf{r}_o}{\|\mathbf{r}_k - \mathbf{r}_o\|} . \tag{24}$$

With these vectors, the angles of longitude θ and latitude β of the unit vector $\mathbf{u}_r$ in the local reference frame are calculated, as depicted in Figure 13a. The angle of maximum amplitude $\beta_{\max}$ is also calculated for a specified longitude θ, using a cubic spline interpolation curve. This curve, uses the angles of maximum amplitude at the four main quadrants (β_{I}, β_{II}, β_{III} and β_{IV}), to interpolate the angle of the maximum amplitude $\beta_{\max}$ for a specified longitude θ, as shown in Figure 13b.

If the effective latitude β exceeds the maximum allowable latitude $\beta_{\max}$, then a penetration on a zone of unacceptable position is occurring and the penalty resisting torque is applied. The magnitude of this torque increases rapidly with the penetration and the direction is the result of the cross-product between vector $\mathbf{u}_\zeta$ and vector $\mathbf{u}_r$:

$$\mathbf{m}_{p_i} = m_{p_i} \left[3 \left(\frac{\beta_i - \beta_{i_{\max}}}{\Delta\beta_i} \right)^2 - 2 \left(\frac{\beta_i - \beta_{i_{\max}}}{\Delta\beta_i} \right)^3 \right] \tilde{\mathbf{u}}_\zeta \mathbf{u}_r , \tag{25}$$

where the term between brackets is a third order curve with the behavior depicted in Figure 14. The direction of the resistance moment depicted in Equation (25) is accurate for circumduction cones with a circular base. Otherwise, the direction of the moment must be set to be tangent to the generalized cone base in the point of contact with $\mathbf{u}_r$.

Table VI describes the values for the limiting angles for the different joints of the human body [3].

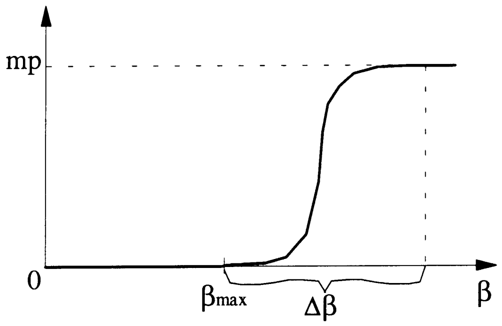

Figure 14. Third order curve.

Table VI. Joint resistance data.

Joint	$\beta_{i_{\mathrm{I}}}$ [°]	$\beta_{i_{\mathrm{II}}}$ [°]	$\beta_{i_{\mathrm{III}}}$ [°]	$\beta_{i_{\mathrm{IV}}}$ [°]	$\Delta\beta_i$ [°]	m_i [g]	m_{p_i} [Nm]	j_i [Nms]
1	40.0	35.0	30.0	35.0	11.5	2.0	226.0	16.950
2	60.0	40.0	60.0	40.0	15.0	2.0	678.0	3.390
3–5	140.0	90.0	30.0	90.0	11.5	1.0	226.0	3.763
4–6	90.0	–	45.0	–	11.5	1.0	226.0	3.390
7–9	10.0	120.0	50.0	45.0	11.5	2.0	452.0	5.650
8–10	–	90.0	–	45.0	11.5	1.0	226.0	5.650
11	19.0	–	2.0	–	15.0	2.0	452.0	16.950

6. Results

The biomechanical model described before, is applied to three case tests. In the first and second examples, a rigid seat model is used in order to support the occupant in a seated position. In the second example, besides the rigid seat, a seat belt model is also used to support the biomechanical model during the impact simulation. In the third case, the interaction between the body segments and the ground is implemented. The *Severity Index* (SI) and the *Head Injury Criteria* (HIC), are also calculated [18].

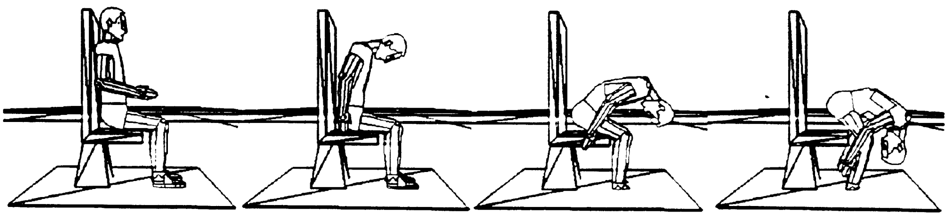

Figure 15. Animation sequence

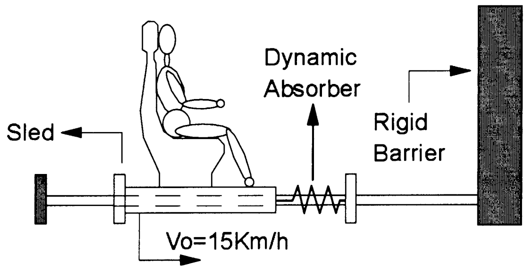

Figure 16. Initial conditions.

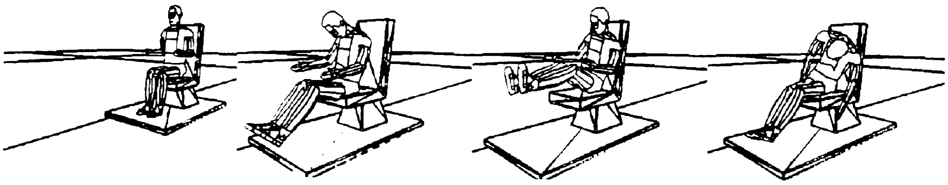

Figure 17. Sequence of animation.

6.1. FORWARD FALL

In this example, the model is seated in a rigid seat. No external forces are applied besides the reactions between the seat and the model and gravity. The results obtained show that the predicted behavior of model is qualitatively similar to the expected movement. In Figure 15, it is observed that the model reaches the maximum allowable motion in several joints. Anytime this happens, the two adjacent segments move together as a single rigid body. This observation is consistent with the human body passive motion.

6.2. FRONTAL IMPACT WITH A RIGID BARRIER

In this example, the biomechanical model is seated in a rigid seat that is mounted on a moving sled, as shown in Figure 16. The sled moves with a closing speed of 15 km/h towards a rigid barrier, until the impact occurs. Two non-linear energy absorbing devices are mounted in the front of the sled. A shoulder-lap seat belt model is used to support the biomechanical model during the simulation.

The animation sequence of the simulation is presented in Figure 17. In this sequence, only the biomechanical model and the seat are described. The seat belt and the rigid barrier are not displayed in the animation. The displacements, velocities and accelerations on each body segment are calculated. In Figure 18, the resultant acceleration on the head and the penalization torque in the neck-torso joint are presented.

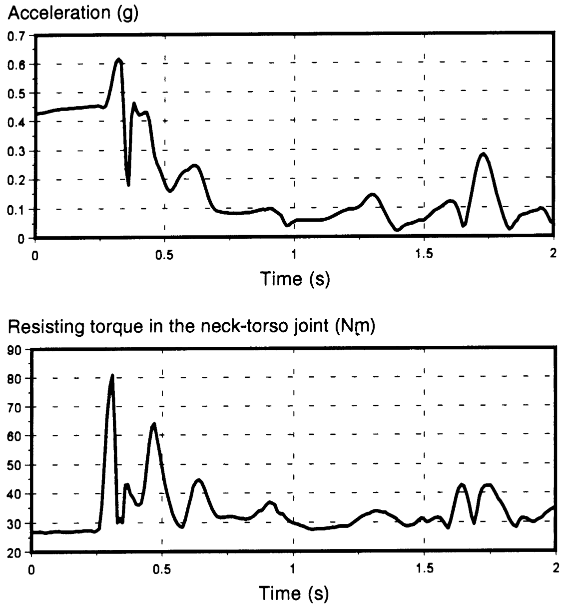

Figure 18. Resultant head acceleration and neck–torso torque.

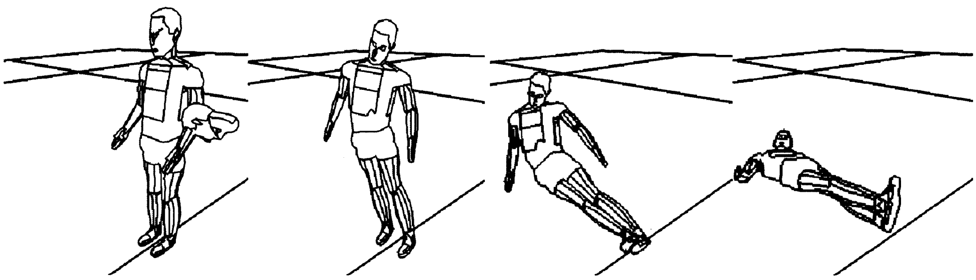

Figure 19. Animation sequence.

6.3. Offside Tackle of an Athlete

In this example, the biomechanical model is applied to the simulation of a player experiencing an offside tackle by another player. The athlete is standing, while the incoming player, with a total mass of 75 kg, is moving forward with a velocity of 3 m/s, as represented in the first frame of the animation sequence in Figure 19.

In the simulation of the tackle, the displacements, velocities accelerations and forces acting upon the body segments are calculated. In particular, the resultant acceleration of the athlete's head is presented in Figure 20. Based on the results of the simulation, an SI value of 2170 and a HIC value of 873 for the injury criteria are calculated. In this case it is suggested that the player would be in the survivability limit due to head injuries.

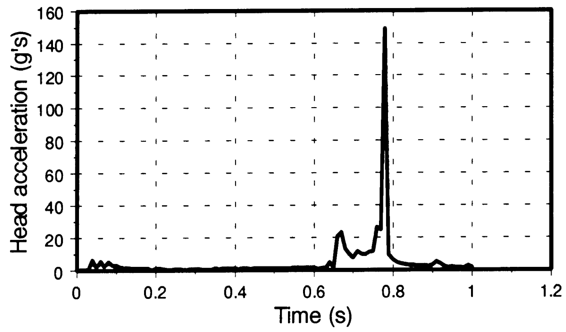

Figure 20. Resultant head acceleration.

7. Conclusions

A biomechanical model based on the SOMLA occupant was developed in this work using natural co-ordinates. The range of motion of the biomechanical segments was kept in a prescribed zone of feasible motion using force penalization terms on the joints anytime the relative position of two adjacent segments started to violate that region. The contact between the biomechanical segments and the surrounding objects or other segments was described by a continuous contact/impact force model. The combined use of the joint resistance and the contact force model results in a numerically stable biomechanical model suitable to be used in a wide variety of scenarios where contact of the human body plays an important role. However, some more investigation is required to identify the relative limits of motion of different biomechanical segments. Also, a better characterization of the mechanical properties of contacting surfaces is necessary. A general purpose database, describing the characteristics of different individuals was developed and related to the program. Finally, the model was applied in different activities that involve body contact. These applications showed that the basic biomechanical models used in crash analysis are still suitable for use in other situations of human body contact provided that the geometry and characteristics of the surfaces in contact are well known.

Acknowledgements

The work presented here was partially supported by the Junta Nacional de Investigação Cientifíca e Tecnológica, JNICT, within the project PRAXIS 3/3.1/CTM/10/94 and by the AGARD project P-77. The authors would like to thank Professor João Abrantes and Dr José Botelheiro for their contribution towards the identification of the range of motion of biomechanical joints.

References

1. Nigg, B.M. and Herzog, W., *Biomechanics of the Musculo-Skeletal System*, John Wiley and Sons, Toronto, 1994.
2. Prasad, P., ‘An overview of major occupant simulation models’, in *Mathematical Simulation of Occupant and Vehicle Kinematics*, SAE publication P-146, SAE paper No. 840855, 1984.
3. Laananen, D., Bolukbasi, A. and Coltman, J., ‘Computer simulation of an aircraft seat and occupant in a crash environment – Volume 1: Technical report’, US Department of Transportation, Federal Aviation Administration, Report No. DOT/FAA/CT-82/33-I, 1993.
4. Laananen, D., ‘Computer simulation of an aircraft seat and occupant(s) in a crash environment – Program SOM-LA/SOM-TA User manual’, US Department of Transportation, Federal Aviation Administration, Report No. DOT/FAA/CT-90/4, 1991.
5. Obergefell, L.A., Gordon, T.R. and Fleck, J.I., ‘Articulated total body model enhancements, Vol. 2: User’s guide’, Report No. AAMRL-TR-88-043, Armstrong Aerospace Med. Research Lab., Wright Patterson Airforce Base, Dayton, Ohio, 1988.
6. TNO,*Madymo User’s Manual, Version 5.0*, TNO, Delft, 1992.
7. Jalón, J.G. and Bayo, E., *Kinematic and Dynamic Simulation of Multibody Systems*, Springer-Verlag, Heidelberg, 1994.
8. Nikravesh, P.E. and Affifi, H.A., ‘Construction of the equations of motion for multibody dynamics using point and joint coordinates’, in *Computer-Aided Analysis of Rigid and Flexible Mechanical Systems*, M.S. Pereira and J.A.C. Ambrósio (eds), Kluwer Academic Publishers, Dordrecht, 1994, 31–60.
9. Nikravesh, P.E., *Computer-Aided Analysis of Mechanical Systems*, Prentice-Hall, Englewood-Cliffs, NJ. 1988.
10. Haug, E.J., *Computer Aided Kinematics and Dynamics of Mechanical Systems*, Allyn and Bacon, Chicago, 1989.
11. Bayo, E. and Ledesma, R., ‘Augmented Lagrangian and mass-orthogonal projection methods for constrained multibody dynamics’, *Journal of Nonlinear Dynamics* **9**, 1996, 113–130.
12. Avello, A. and Bayo, E., ‘A singularity-free penalty formulation for the dynamics of constrained multibody systems’, *Mechanical Design and Synthesis, ASME* **DE-Vol. 1**, 1992, 643–649.
13. Gear, C.W., ‘Numerical solution of differential-algebraic equations’, *IEE Transactions on Circuit Theory* **CT-18**, 1981, 89–95.
14. Lankarani, H., Ma, D. and Menon, R., ‘Impact dynamics of multibody mechanical systems and application to crash responses of aircraft occupant/structure’, in *Computational Dynamics in Multibody Systems*, M.F.O.S. Pereira and J.A.C. Ambrósio (eds), Kluwer Academic Publishers, Dordrecht, 1995, 239–265.
15. Love, A.E.H., *A Treatise on the Mathematical Theory of Elasticity*, 4th edition, Dover Publications, New York, 1944.
16. Silva, M.S.T and Ambrósio, J.A.C., ‘Modelo Biomecânico Para A Dinâmica Computacional Do Movimento Humano Articulado’ (Biomechanical model for the computational dynamics of the human articulated motion), Technical Report IDMEC/CPM-96/003, IDMEC – Instituto Superior Técnico, 1996.
17. CIBA GEIGY, *Folia Rheumatologica, Motilität von Hüfte, Schulter, Hand und Fuß*, CIBA GEIGY GrubH Wehr/Baden, 1979.
18. Wismans, J.S., Janssen, E.G., Beusenberg, M., Koppens, W.P. and Lupker, H.A., ‘Injury biomechanics’, Third term W-3.3, WMT-3.3, code 4J610, Faculty of Mechanical Engineering, Eindhoven University of Technology, 1994.